

# Design of a fully modular and backdrivable dexterous hand

Javier Martin<sup>1</sup> and Mathieu Grossard<sup>2</sup>

## Abstract

This paper presents the mechatronic design of a new anthropomorphic hand. It has been developed in the context of a multidisciplinary project which aims at understanding how humans perform the manipulation of objects in order to replicate grasping and in-hand movements with an artificial hand. This has required the development of a new hand with a high level of both anthropomorphism and dexterity. The hand must exactly replicate the kinematics of the human hand, adding up to 24 degrees of mobility and 20 degrees of freedom, which is a design challenge if a high level of dexterity must be guaranteed. Three key concepts have guided the mechanical design: modularity, backdrivability and mechanical simplicity. A modular approach simplifies the complex hand assembly and permits us to concentrate our efforts on one basic unit which will be replicated throughout the hand. Mechanical simplicity and backdrivability ensure a good natural mechanical behavior, essential for stable control of contact forces. Likewise, a better controllability will enhance the dexterity of the hand. A thorough mechanical design assures backdrivability through the whole mechanism, including actuators and transmission of movement to the joints. Experimental results confirm the validity of the design approach and will open new lines of research into robotic hands.

## Keywords

Hand design, backdriveable mechanics, tendon-driven actuation, kinematics

## 1. Introduction

When dealing with the design of robotic hands, anthropomorphism and dexterity appear as orthogonal concepts whose reciprocal dependence has not yet been proved (Melchiorri and Kaneko, 2008). On the one hand, anthropomorphism relates to the external perceivable properties, for which the cited work proposes several indicators such as kinematics, contact surfaces and size. Anthropomorphism is a consistent design driver when the designed robotic hand is intended to be used in a human-oriented environment, or it aims at directly reproducing an operator's hand behavior as a teleoperated end-effector, or if a human-like aspect is desired, for example in humanoid robots, assistance robots or prosthetic devices. However, human-like hands present some drawbacks such as complex kinematic structure, a high number of actuators and sophisticated sensing systems (Bicchi, 2000).

On the other hand, dexterity refers to the capability of changing the position and orientation of a manipulated object from a given reference configuration to a different one, arbitrarily chosen within the hand workspace. Dexterity is related to both the mechanical structure and the sensory apparatus of the robotic hand, and it is the

most important indicator of its actual functionality. Melchiorri and Kaneko (2008) distinguish two main areas in the dexterity domain: grasping (Cutkosky, 1989) and in-hand manipulation or internal manipulation (Bicchi, 2000).

Related to dexterity, an important characteristic of robotic hands is the compliance, which allows the fingers to better adapt to the grasped object. Furthermore, adjustable compliance enables human-like soft grasping by the robotic hand (Jau, 1995), and is one of the most important quantities for characterizing the grasp of an object (Kazerooni et al., 1986; Goldenberg, 1988; Cutkosky and Kao, 1989; Jung et al., 1999; Doulgeri and Arimoto, 2002; Doulgeri and Karayannidis, 2005), particularly in fine manipulation. In addition to all these functionality aspects, compliant hands are intrinsically safer and better protected against unexpected external impacts. This is of particular interest in service and humanoid robotics, where hands are

<sup>1</sup>Centro Universitario de la Defensa, Spain

<sup>2</sup>CEA, LIST, Interactive Robotics Laboratory, France

### Corresponding author:

Javier Martin, Centro Universitario de la Defensa, Ctra. de Huesca s/n, 50090 Zaragoza, Spain.  
E-mail: j.martin@unizar.es

expected to be able to interact safely with a priori unknown environments, objects or humans.

These aspects have become the object of numerous research activities (Salisbury and Craig, 1982; Salisbury and Roth, 1983; Baker et al., 1985; Kerr and Roth, 1986; Okada, 1986; Hanafusa and Asada, 1997; Bitzer and Smagt, 2006; Martell and Gini, 2007; Chalon et al., 2010; Grebenstein et al., 2010b; Chalon et al., 2011), and an increasing number of robotic hands have been developed for research and industry (Salisbury and Ruoff, 1981; Jacobsen et al., 1986; Maekawa et al., 1992; Fischer and Woern, 1998; Ambrose et al., 2000; Hirzinger et al., 2000; Butterfaß et al., 2001; Gazeau et al., 2001; Kawasaki et al., 2002; Namiki et al., 2003; Yamano et al., 2003; He et al., 2004; Roccella et al., 2004; Hoshino and Kawabuchi, 2005; Lotti et al., 2005; Matsuoka et al., 2006; Kaneko et al., 2007; Liu et al., 2008; Dollar and Howe, 2010; Ueda et al., 2010; Grebenstein et al., 2012; ShadowRobotCompany, 2013). However, it remains a difficult and unsolved problem to address all these requirements in a single device. To name a few examples, the hand of the DLR Hand Arm System (Grebenstein et al., 2012) is a 19-degrees-of-freedom (DoF) hyperactuated anthropomorphic hand with a highly robust design based on variable stiffness actuators. Such actuators provide an effective protection from external impacts and allow stiffness adjustments depending on the task. Dollar and Howe (2010) present a highly adaptive non anthropomorphic hand with few sensors and a single motor. It is capable of picking up a wide variety of objects thanks to passive joint compliance; however, limited to power grip. The Dexterous Hand by Shadow Robot Company Ltd achieves the highest level of anthropomorphism with 24-DoF which exactly replicate those of the human hand (ShadowRobotCompany, 2013), based on either pneumatic muscles or DC motors.

In short, numerous design approaches can be found in the literature, both at the hardware and control level. The authors believe there is still room for improvement exploiting the concept of backdrivability (Koganezawa et al., 2011). A mechanism is defined as backdrivable when motion can be transmitted both from the input to the output and vice versa. The implications of backdrivable mechanics on control, sensing and safe interaction with the environment are further discussed in Section 2.2.

This work presents a novel fully modular and backdrivable hand, the CEA dexterous hand (Figure 1), as a partial result of a multidisciplinary research project integrating neuroscience, developmental psychology, cognitive science, robotics, multimodal perception and machine learning. The aim of the project is to understand how humans perform the manipulation of objects in order to replicate grasping and skilled in-hand movements with an artificial hand. In this context, a new robotic hand has been designed which attempts to achieve high levels of both anthropomorphism and dexterity.



**Fig. 1.** The CEA dexterous hand.

This paper is organized as follows. In section 2, the design rationale of the CEA dexterous hand is outlined. Section 3 describes the design and modeling of a basic mechanical module, the three-axes unit, which is then reproduced in all fingers and the thumb. Section 4 presents experimental studies on a finger of the new hand. Finally, conclusions and future lines of work are summarized.

## 2. Mechanical design rationale, tradeoffs and implications on control, sensing and safety

Figure 1 shows the CEA dexterous hand. It provides five fingers with four joints each and five joints for the thumb, the flexion of the palm and the wrist flexion/extension, amounting for a total of 20 actuated DoF and 24 degrees of mobility. All DoF are driven by specially designed backdriveable actuators, achieving a fingertip force of 4.2 N. It integrates the actuators, miniaturized power boards, low-level control algorithms for the position/torque of the joints and an interface with the ROS environment. The actuators are embedded in the palm and thumb base and the electronic power boards and low-level controller are embedded in the forearm to facilitate the connection of the hand on any robotic arm. The maximum electric power consumption of the overall system is 168 W and total weight of the complete hardware is 4.2 kg.

The kinematic structure of the complete hand (Figure 2) exactly replicates that of the Shadow Hand (ShadowRobotCompany, 2013), being the Shadow Robot Company the industrial partner in the project which supports this work. The reason for this design choice is that the project needed

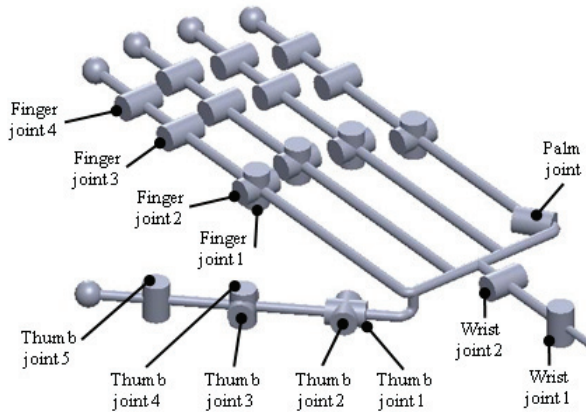


**Fig. 2.** Kinematics of the artificial hand.

an anthropomorphic robotic hand, able to exactly replicate the recorded movements of a human hand. In this respect, the kinematic structure of the Shadow Hand is recognized as a gold standard in terms of anthropomorphism. It comprises five fingers with four joints each and five joints for the thumb, the flexion of the palm and the wrist flexion/extension.

Regarding the term ‘anthropomorphism’, as previously explained (Biagiotti et al., 2004) proposes an anthropomorphism index that is calculated as the weighted sum of three aspects: kinematics, contact surfaces and size (see the cited work for a more detailed explanation on each aspect and the weighting coefficients). Further on in the text it will be explained that, due to the design choices, the palm and the portion of the thumb base which is opposed to the palm are considerably thicker than their counterparts in the human hand. Therefore, our hand is highly anthropomorphic regarding only the kinematics and contact surfaces involved in in-hand manipulation. The rest of the aspects accounted for in the anthropomorphism index have been sacrificed in a design trade-off to maximize dexterity.

It must be clarified that, even if the kinematic structure of the Shadow Hand has been taken as the starting point of the new CEA hand, both hands are completely different regarding actuation technology, tendon routing and in general design rationale.

The complete kinematic structure of the CEA dexterous hand can be summarized as follows:

- Fingers: four degrees of mobility and three DoF. The distal and medial phalanges are kinematically coupled with a constant ratio between both rotation angles;
- Thumb: five DoF;
- Palm: one additional degree of freedom at the basis of the little finger;
- Wrist: two DoF.

### 2.1. Modularity

A modular design approach brings forward several advantages, such as simplification of the hand assembly, simplification of the hand maintenance, performance homogeneity

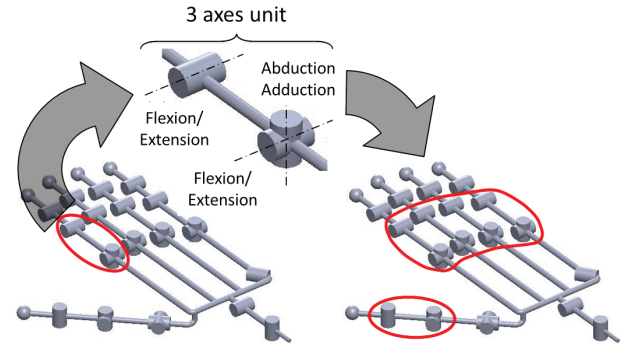


**Fig. 3.** The modular approach in the context of the hand structure design.

and the possibility of having different hand configurations with a different number of fingers or combination of fingers and thumb, for example. Thus, a modular approach has been taken which consists in focusing on the optimal solution of the *three-axes unit*. The three-axes unit is a separable three-DoF sub-mechanism with its associated actuators and transmission, which is common to all the fingers and the thumb (Figure 3). It consists of a serial combination of abduction/adduction, flexion/extension and flexion/extension, where the axes of the abduction/adduction and the first flexion/extension intersect. Each three-axes unit is controlled by one independent and integrated electronic architecture combining the low-level control part and power board, allowing for the control in position, speed and torque modes for each joint. The main interest of the three-axes unit is that it permits the combination of complex kinematics with a modular approach. A detailed description of the unit is given in section 3.

### 2.2. Backdrivability

As above explained, a mechanism is defined as backdriveable when motion can be transmitted both from the input to the output and vice versa. Impediments to backdrivability are friction and inertia in the mechanism; as a consequence, backdrivability is a difficult goal which requires a careful and fine design of both actuators and mechanical power transmission. For the actuation of the 20 DoFs, backdriveable actuators have been specially designed, based on a rotary DC motor coupled to a ball-screw rotary-to-linear transmission. A more detailed description will be given in Section 3.1. Next, advantages and design tradeoffs associated with mechanical backdrivability are discussed.

First, it permits a single-acting actuation architecture with passive return (Melchiorri and Kaneko, 2008), which greatly simplifies tendon routing and therefore reduces friction. Note that friction associated with force transmitting tendons is by far the major source of friction in complex mechanical hands (Jacobsen et al., 1986). Nevertheless, this

architecture has a tradeoff between the explained advantages and the possible drawbacks related to the loss of available power for the grasp and the limited response bandwidth in case of low spring stiffness.

Backdrivability is essential for good natural mechanical behavior by permitting accurate feed-forward force control in the face of disturbances (Townsend and Salisbury, 1989) and for stable control of contact forces. Regarding simple impedance control, which is the most widely used control approach when physical interaction is intended with robots (Albu-Schäffer et al., 2008; Haddadin et al., 2011), stability and performance get better as the inherent robot impedance decreases. For this reason, this type of controller performs particularly well when used in conjunction with highly backdrivable devices which inherently have low inertia and low friction (Hogan, 1985). In our case, the resulting mathematical model of the physical behavior of the finger enables alternative strategies to control the mechanical compliance at the contact point (Martin et al., 2011). Thus, backdrivability is an important advantage for the control. We have to take into account that (Biagiotti et al., 2004) state that dexterity of a robot hand is the result of its mechanical structure as well as of its sensory equipment; but an estimate of the real dexterity has to take into account the intelligence, that is the control. Thus, as backdrivability enables a better control of the mechanism, it ultimately enhances the real dexterity of a robot hand.

Another advantage of backdrivability is that it enables the measurement of tendon forces by the resistive torque induced on the DC motor shaft, using a measure of the motor current. This is possible as the image of the tendon forces, seen from the motors, is not much degraded by the low mechanical impedance of the transmission. Then, using the coupling matrix it is possible to obtain an estimate of the joint torques. Furthermore, if the contact point is located by an additional sensing technology, it is possible to obtain an estimate of the contact forces (explained in more detail in Section 4.3.2). This feature greatly improves the sensory capabilities of the hand: every surface becomes sensitive as every part of the hand is driven by a backdrivable actuator. Let us note the proposed approach only requires the contact point information from a complementary additional sensing technology. This could be provided by a tactile skin with only good spatial resolution (even with limited or in-existing force sensitivity).

Although the most straightforward way of estimating the external forces is to use an exteroceptive force or tactile sensor (Albu-Schäffer et al., 2007), our approach is particularly relevant if we recall that tactile sensing is a not yet solved problem. Although tactile sensor technology has reached quite a level of maturity, currently available sensors cannot handle the tactile sensing requirements of robotic hands intended for advanced and in-hand manipulation. Existing sensor technologies can provide only a small subset of the needed tactile sensory information (e.g. limited

force range, insufficient spatial and temporal resolution, limited sensing area and limited capability of sensing shear forces) (Yousef et al., 2011). Thus, our mechanic design rationale is a complementary solution that could help compensate for the technical difficulty of realizing a sufficiently functional artificial skin. This is a truly interdisciplinary approach to the design of sensitive artificial hands for in-hand manipulation. Naturally, a tradeoff exists between the improved sensitivity and the system complexity. However, when positioning our approach in that tradeoff space it has to be taken into account that we have significantly reduced the system complexity by simplifying the mechanics and reducing the need for tendon force sensors.

Backdrivability is also an advantageous feature from the perspective of safety and robustness, as it provides a natural protection against unexpected external impacts. When using an impedance controller, the mechanical stiffness prevails at very short timescales, and in the slow timescale the overall behavior is given by the combination of mechanical and controller stiffness (Grebenstein et al., 2012). Thus, during an impact, the physical stiffness of the robot equals its mechanical stiffness at least during the first control cycle: a stiff robot using active compliance appears stiff in case of collision (Grebenstein et al., 2011). A backdrivable robot has an inherent low mechanical impedance; therefore it will display a low impedance in the case of collision. It must be clarified that backdrivability is not the only valid approach to safety, as it will appear when contrasting the CEA hand with the DLR hand in Section 3.8.

The reduction ratio  $N$  introduced by the ball-screw in the actuator causes the inertia of the DC motor to be reflected at the joint, amplified by a factor of  $N^2$ . Therefore, a high value of  $N$  would cause the reflected motor inertia to dominate the total inertia measured at the joint and thus degrade the acceleration-dependent backdrivability (Townsend and Salisbury, 1989). With this design guideline, a higher output motor was chosen with a lower value of  $N$ , which implies a bigger DC motor. Dimensions of the actuators for the required force output prevent their integration in the phalanxes, therefore they need to be placed in the palm/forearm, which results in a loss of anthropomorphism regarding the thickness of the palm. However, we achieve an improvement of the backdrivability in terms of low inertia of the moving parts and the size and slenderness of the fingers remain completely anthropomorphic. Therefore it is a design tradeoff which might hinder some tasks requiring the palm to go through narrow spaces, but it enhances in return the majority of in-hand manipulation tasks.

### 2.3. Mechanical simplicity

As above explained, a high level of anthropomorphism always implies more complex mechanical structures with large number of DoF, actuators and sensors and more complex control strategies. Complex mechanics are more prone

to bringing forward several disadvantages such as coupling between DoFs, additional friction and backlash, non-desired compliance and complex dynamics that compromise the actual dexterity of the hand. Therefore, a careful design is required to minimize these disadvantages by providing the simplest mechanical arrangement. This is key to enabling better controllability of the mechanism and thus improved dexterity of the hand.

The first simplification is to arrange the whole kinematic structure exclusively with revolute pairs (see Figure 1). The second simplification is a key design feature of the CEA dexterous hand: its simplified tendon routing. Actuator backdrivability makes it possible to design a novel tendon routing which minimizes the number of tendons and kinematic and static coupling between the different axes in the three-axes unit. To that regard, independent joint control is a desired target since it allows a decoupled analysis of the closed-loop system using single-input/single-output (SISO) classical control schemes. This simplification of the control is relevant in practical implementations, due to the complexity of multi-input/multi-output (MIMO) control schemes. Besides, the proposed tendon routing also minimizes the number of idle pulleys and direction changes in the tendon routing, which in turn minimizes overall friction. This simplification of the mechanics improves the overall backdrivability of the actuation and transmission as a whole. A detailed description and modeling of the tendon routing is provided in Section 3.2.

### 3. Basic module: Design of the three-axes unit

#### 3.1. Backdriveable actuators

The operation of the specially designed backdrivable actuators is briefly described as follows: first, a DC electrical motor transmits a rotational movement to a ball-screw in which the nut has been locked in rotation but left free to displace along its axis (Figure 4). The induced displacement of the nut is then transmitted to a tendon which finally drives a rotational joint. For high pitch-to-radius ratios, this actuator shows a good backdrivability.

DC motors have been chosen to power the actuation system due to their simplicity of operation and current measurement, and the same motor has been chosen for all the actuators to simplify electronics, design and integration.

Using a Maxon Motor RE16 coupled to a Steinmeyer Type B ball-screw of 3 mm diameter, 1 mm pitch, and an integrated block-and-tackle mechanical amplification, an output force of 60 N has been achieved with a backdrivability threshold of 4 N (at the actuator output). The no-load maximum linear velocity is 0.021 m/s and a linear position resolution of 0.001 mm is obtained by coupling a Maxon Encoder MR, Type M, 512 cpt to the motor. Two different versions of the actuator have been built, mono-directional to actuate the flexion/extension DoFs in opposition to passive return elements (Figure 4a), and bi-directional to actuate the remaining DoFs (Figure 4b).

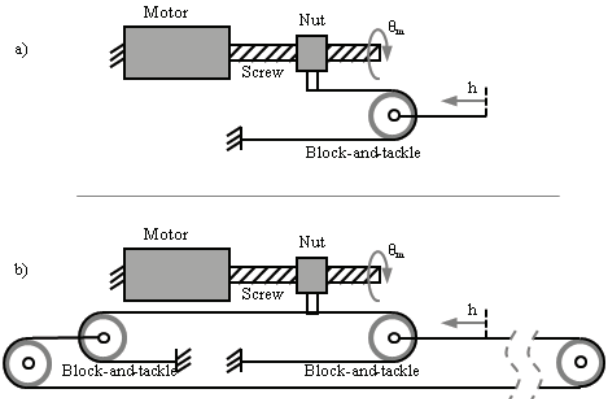


**Fig. 4.** Schematic description of the actuation principle common to all actuated DoFs of the CEA hand, being used in two versions: (a) mono-directional and (b) bi-directional

The kinematic relationship between the rotation of the motor  $\theta_m$  and linear displacement at the actuator output  $h$  is given by:

$$h = \frac{P}{4\pi} \theta_m \quad (1)$$

where  $P$  is the pitch of the ball-screw.

#### 3.2. Transmission and tendon routing

The 3-axes unit consists of a serial combination of abduction/adduction (axis 1, angle  $\theta_1$ ), flexion/extension (axis 2, angle  $\theta_2$ ) and flexion/extension (axis 3, angle  $\theta_3$ ), where axes 1 and 2 intersect. Axis 1 is driven with a double-acting actuation architecture and axes 2 and 3 are driven with a single-acting actuation architecture with passive return elements. All actuators are packed together upstream axis 1 and the movement is transmitted by tendons to all axes. A description of the three-axes unit can be summarized as follows (Figure 5):

- Axis 1 is driven by actuator 1 acting on pulley  $r_1$  with cable 1.
- Axis 2 is driven in the flexion movement (positive  $\theta_2$ ) by actuator 2 acting on pulley  $r_2$  with cable 2, which passes through idle pulley  $r_{2'}$ . By construction, the tangency point where cable 2 leaves idle pulley  $r_{2'}$  always lies on axis 1. Axis 2 is driven in the extension movement (negative  $\theta_2$ ) by spring  $k_2$ . Spring  $k_2$  is attached to link 1 by a cable which winds up on a pulley with radius  $r_{s2}$ , and is attached to link 2 at a distance  $r_{s2}$ .
- Axis 3 is driven in the flexion movement (positive  $\theta_3$ ) by actuator 3 acting on pulley  $r_{3b}$  with cable 3, which passes through idle pulleys  $r_{3'}$  and  $r_{3a}$ . The tangency point where cable 3 leaves idle pulley  $r_{3'}$  always lies on axis 1. Axis 3 is driven in the extension movement (negative  $\theta_3$ ) by spring  $k_3$ . Spring  $k_3$  is attached to link 1 by a cable which winds up on a pulley with radius  $r_{s3}$ , and is attached to link 3 by a cable which winds up on a pulley with radius  $r_{s3}$ ;

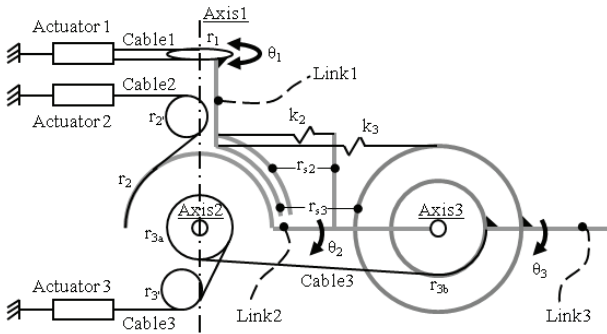


**Fig. 5.** Schematic description of the three-axes unit.

- The three actuators stay fixed. Pulleys  $r_2'$ ,  $r_3'$  and the portion of cables 2, 3 connecting the actuators with pulleys  $r_2'$ ,  $r_3'$  stay always in the same plane. The rest of the mechanism (pulleys, cable portions and springs) is contained in a plane which pivots around axis 1 by an angle  $\theta_1$ .

The advantages of this mechanism are summarized next:

- The total length of cables 2, 3 remains unchanged as the mechanism undergoes a rotation  $\theta_1$  around axis 1. This prevents kinematic coupling between abduction/adduction movements and flexion/extension movements. This stands for small values of  $\theta_1$ , which is the case in the intended application of the hand.
- No extra pulleys are needed to pass cables 2, 3 through axis 1 (which is a classical problem in tendon routing for mechanical hands), even if axes 1 and 2 intersect.
- Equivalent joint stiffness provided by springs 2, 3 for the extension movement remains constant. This simplifies the control of the hand.
- Since springs 2, 3 are set to connect two orthogonal axes, there is no static coupling between Abduction/adduction movements and flexion/extension movements due to reactions in the links.
- Since springs 2, 3 do not pass through axis 1 to get to the fixed frame (as is usual in many designs), there is no kinematic coupling between axis 1 and axes 2, 3 due to the routing of springs.
- Since spring 3 is set to connect links 1 and 3 without passing through link 2, there is no additional coupling between axis 2 and 3 due to cable routing. Since spring 3 is attached to pulleys of equal radius  $r_{3a}$ , there is no additional static coupling due to the propagation through link 2 of the spring force applied to axis 3.
- The cable arrangement minimizes free lengths of all cables (a few centimeters maximum). This avoids undesired compliance of the cable transmission.

It is important to note the only coupling in this mechanism is the kinematic coupling between  $\theta_2$  and  $\theta_3$ , due to the non-zero radius of pulley  $r_{3a}$ . Such coupling could be removed reducing the radius of pulley 3a to zero, reducing

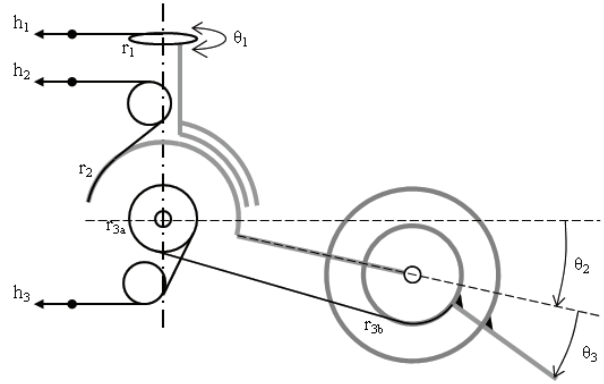


**Fig. 6.** Tendon transmission connecting actuators with joints.

the pulley to a fulcrum placed in the intersection between axes 1 and 2. However, there would always exist a residual kinematic coupling as it is not possible to obtain a perfect fulcrum in practice. Moreover, a fulcrum would introduce excessive friction which would be detrimental for single-acting architecture and the backdrivability of the actuation. In the same direction, minimizing the number of idle pulleys and direction changes in the cable routing further minimizes overall friction in the mechanism. To sum up, controllability of the hand is greatly improved by the mechanical design advantages: minimum friction, minimum coupling between DoFs, simplified joint stiffness models and avoidance of undesired sources of compliance.

### 3.3. Kinematic and static modeling of the tendon transmission

In this section we describe how forces applied by the actuators and the springs are related to the joint torques applied to the mechanism. We will use the procedure and notation proposed by Murray et al. (1994), where both elastic and inelastic tendons are considered.

First, we will model the transmission of actuator forces through inelastic cables (Figure 6).

The routing of each tendon is modeled by an extension function  $h_i$  which measures the displacement of the end of the tendon as a function of the joint angles of the finger (positive when tendons are extended, negative when tendons are contracted). The vector of tendon extensions is given by

$$h = \begin{pmatrix} l_{1,0} - r_1\theta_1 \\ l_{2,0} - r_2\theta_2 \\ l_{3,0} - r_{3a}\theta_2 - r_{3b}\theta_3 \end{pmatrix} \quad (2)$$

The coupling matrix is calculated as

$$P(\theta) = \frac{dh^T}{d\theta} = \begin{pmatrix} -r_1 & 0 & 0 \\ 0 & -r_2 & -r_{3a} \\ 0 & 0 & -r_{3b} \end{pmatrix} \quad (3)$$

and using conservation of energy

$$\tau_{act} = P(\theta)f \quad (4)$$

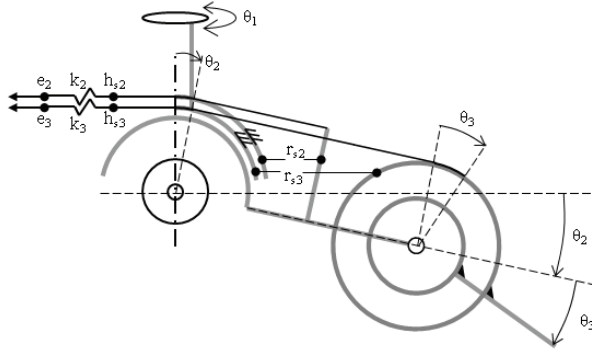


**Fig. 7.** Tendon transmission connecting return springs with joints.

where  $\tau_{act}$  is the vector of joint torques and  $f$  is the vector of forces applied by the actuators to the ends of the tendons. According to the sign criteria,  $f > 0$  when they cause the tendons to be extended,  $f < 0$  when they cause the tendons to be contracted. Actuator 1 is double-acting; hence  $f_1$  can be positive or negative. Actuators 2, 3 are single-acting; therefore it will always be  $f_2, f_3 < 0$  as actuators can only pull on the tendons.

Second, we will model the transmission of spring forces as elastic cables. Figure 7 shows an equivalent model of the real mechanism that complies with the modeling methodology proposed by Murray et al. (1994). In this equivalent model (not in the real mechanism), we assume that the tendons are completely free to slide along the pulleys of radius  $r_{s2}, r_{s3}$  in link 1 without friction, and hence we can lump all elasticity into a single spring element at the base of the tendon.

Extension functions are given by

$$h_s = \begin{pmatrix} 0 \\ l_{s2,0} + r_{s2}\theta_2 \\ l_{s3,0} + r_{s3}\theta_2 + r_{s3}\theta_3 \end{pmatrix} \quad (5)$$

The coupling matrix is calculated as

$$P_s(\theta) = \frac{dh_s^T}{d\theta} = \begin{pmatrix} 0 & 0 & 0 \\ 0 & r_{s2} & r_{s3} \\ 0 & 0 & r_{s3} \end{pmatrix} \quad (6)$$

The stiffness matrix is

$$K = \begin{pmatrix} 0 & 0 & 0 \\ 0 & k_2 & 0 \\ 0 & 0 & k_3 \end{pmatrix} \quad (7)$$

Elongation of the tendons is given by

$$h_s(\theta) - h_s(0) = \begin{pmatrix} 0 & 0 & 0 \\ 0 & r_{s2} & 0 \\ 0 & r_{s3} & r_{s3} \end{pmatrix} \begin{pmatrix} \theta_1 \\ \theta_2 \\ \theta_3 \end{pmatrix} \quad (8)$$

The force applied by the springs to the tendons is given by

$$f = K(e + h_s(0) - h_s(\theta)) \quad (9)$$

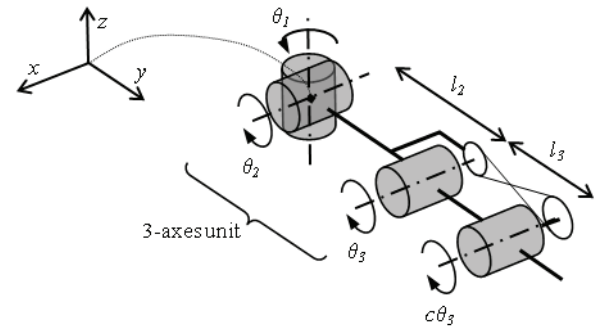


**Fig. 8.** Kinematic structure of a complete finger integrating the three-axes unit.

where  $e$  in our case is a constant value fixed by design, that is the preload of the springs measured as the initial elongation.

$$e = \begin{pmatrix} 0 \\ e_{2,0} \\ e_{3,0} \end{pmatrix} \quad (10)$$

Following the sign criteria, it is a negative value.

The spring force applied to the tendons is related to joint torques by

$$\tau_{spr} = P_s(\theta)(K(e + h_s(0) - h_s(\theta))) \quad (11)$$

Finally, superposing the effects of actuator forces and spring forces, the net joint torques are given by  $\tau = \tau_{act} + \tau_{spr}$

$$\tau = P(\theta)f + P_s(\theta)(K(e + h_s(0) - h_s(\theta))) \quad (12)$$

All geometric parameters are optimized in order to maximize the force output of the three-axes unit when integrated into the fingers, as well as the range of directions along which forces can be exerted taking into account the restriction given by  $f_2, f_3 < 0$ .

### 3.4. From the three-axes unit to the finger

A complete finger can be formed by a three-axes unit plus an additional distal flexion which is mechanically coupled to axis 3. Such coupling consists in a constant ratio  $c$  between the angles rotated by the last two phalanges. This results in a deterministic mechanism with four degrees of mobility and three DoF, shown in Figure 8.

A geometrical description of the mechanism is given by the twist motions for each joint

$$\xi_1 = \begin{pmatrix} 0 \\ 0 \\ 0 \\ 0 \\ 0 \\ 1 \end{pmatrix} \quad \xi_2 = \begin{pmatrix} 0 \\ 0 \\ 0 \\ 0 \\ -1 \\ 0 \\ 0 \end{pmatrix}$$

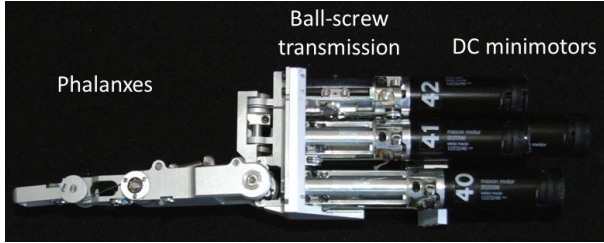


**Fig. 9.** Prototype of the three-axes unit.

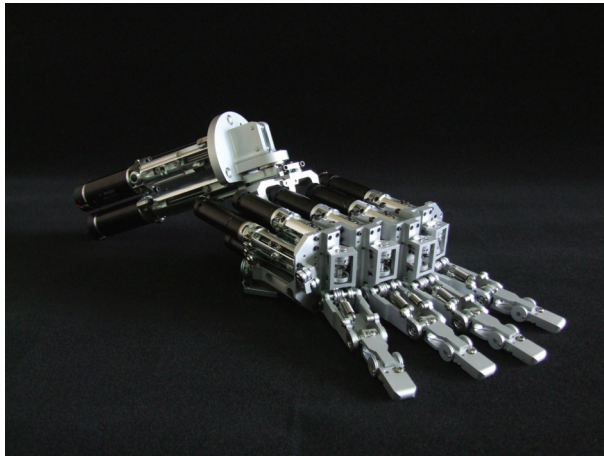


**Fig. 10.** Assembly of the fingers; all actuators are integrated in the palm.

$$\xi_3 = \begin{pmatrix} 0 \\ 0 \\ l_2 \\ -1 \\ 0 \\ 0 \end{pmatrix} \quad \xi_4 = \begin{pmatrix} 0 \\ 0 \\ l_2 + l_3 \\ -1 \\ 0 \\ 0 \end{pmatrix} \quad (13)$$

together with the transformation between the base frame and the frame corresponding to each phalanx at  $\theta = 0$ . Calculation of the forward kinematics and Jacobian matrix is then straightforward following the methodology explained in Murray et al. (1994).

By virtue of the modular approach used for the design of the future hand, the design of a working finger immediately permits us to replicate it four times to form the four fingers of the hand. Figure 9 shows a prototype of the finger and Figure 10 shows the complete assembly of four fingers with an additional one DoF accounting for the palm.

### 3.5. From the three-axes unit to the thumb

The thumb is considered as a three-axes unit mounted at the distal end of a two-DoF pointing mechanism. Thus, the pointing mechanism is in charge of correctly orienting the three-axes unit in order to oppose it to the fingers. The actuators of the three-axes unit are embedded in the pointing mechanism of the thumb, therefore the output of the pointing mechanism actuators needs to be amplified, i.e. by means of a larger pulleys' radius, in order to counteract

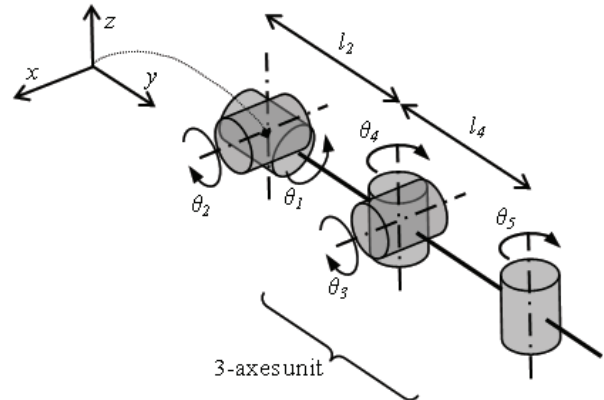


**Fig. 11.** Kinematic structure of the thumb integrating the three-axes unit.

the reactions generated by the actuation of the three-axes unit. This results in a mechanism with five DoF, shown in Figure 11.

A geometrical description of the mechanism is given by the twist motions for each joint

$$\begin{aligned} \xi_1 &= \begin{pmatrix} 0 \\ 0 \\ 0 \\ 0 \\ 1 \\ 0 \end{pmatrix} & \xi_2 &= \begin{pmatrix} 0 \\ 0 \\ 0 \\ -1 \\ 0 \\ 0 \end{pmatrix} & \xi_3 &= \begin{pmatrix} 0 \\ 0 \\ l_2 \\ -1 \\ 0 \\ 0 \end{pmatrix} \\ \xi_4 &= \begin{pmatrix} -l_2 \\ 0 \\ 0 \\ 0 \\ 0 \\ -1 \end{pmatrix} & \xi_5 &= \begin{pmatrix} -l_2 - l_4 \\ 0 \\ 0 \\ 0 \\ 0 \\ -1 \end{pmatrix} \end{aligned} \quad (14)$$

together with the transformation between the base frame and the frame corresponding to each phalanx at  $\theta = 0$ . Calculation of the forward kinematics and Jacobian matrix is then straightforward following the methodology explained in Murray et al. (1994). Figure 12 shows the complete assembly of four fingers plus the thumb.

### 3.6. Embedded electronics

The electronics have been designed to be embedded inside the robotic forearm so as to minimize wires and connectors to achieve a truly autonomous hand that can easily be connected to a robotic arm. The external wires have been limited to the communication and power buses. This hardware includes power electronics, sensor interfaces, power supply, Ethernet connection for communication and Digital Signal Processors (DSPs) that can process the low-level control of the hand and provide an external PC with all the data at a high communication rate.

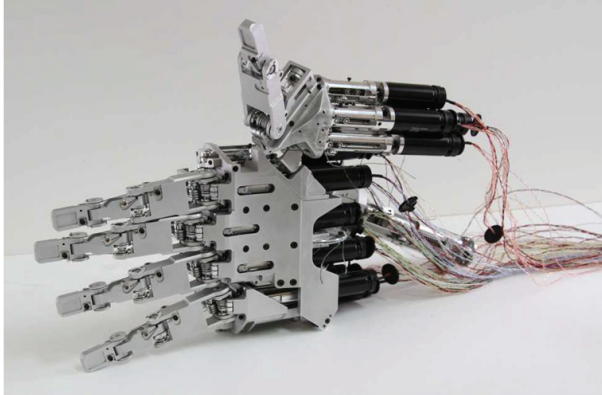


**Fig. 12.** Assembly of the fingers and thumb.

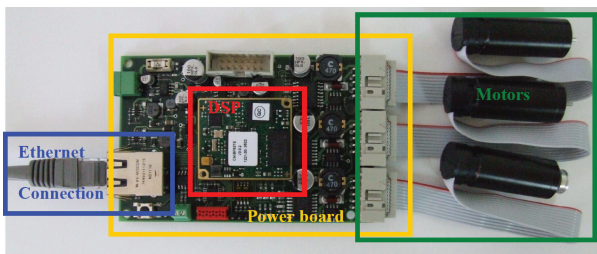


**Fig. 13.** Picture of an elementary electronic board with its main modules: communication interface with the host-PC, power board, Digital Signal Processor (DSP Blackfin BF537) for controlling the three mini-motors of one three-axes unit.

Following the design rationale of the new hand as described previously, the three-axes unit is controlled with a dedicated electronic power board along with its low-level control algorithm (Figure 13).

The placement of the different components on the electronic board has been optimized to minimize the overall dimensions of the board ( $100 \times 65 \times 15$  mm). The system is composed of a DSP mounted on a power electronics board prototype, allowing the control of the DC motors through a cascaded loop scheme presented in the next section. Each power board embeds the three full bridges for the PWM generations, three counters for position, one ADC for the three current measurements and conversions, one Ethernet entry, one power supply and one DSP. Complementing the first 15 active DoF with the 5 active extra degrees relating to the thumb and the palm, the future hand comprises a minimal number of 7 embedded DSPs to perform the control of the whole system. A protocol enables the communication tasks and exchange data between the embedded low-level control and host-PC side running the Robot Operating System (ROS) framework (Dias et al., 2012).

### 3.7. Hand controller

Force and position control modes have been implemented for the CEA dexterous hand. At the lowest level, all control modes close the loop around the error between the

desired actuator torque and the sensed torque. In each case, the inner torque control loop regulates the current passing through the DC mini-motor at a sample time of  $T_e = 40 \mu\text{s}$ . Real currents are estimated from the overall measured voltage passing through the shunt resistor in series with each DC motor. Torque control at the motor level uses a Proportional Integrator controller whose gains are tuned to limit overshoots and avoid static error. Besides, when selecting joint position mode, the controller of each DC motor is based on a Proportional Derivative control law for the outer loop, and will imply the whole cascaded loops process.

As mentioned in Hogan (1985), let us note that driving an intrinsically low-friction mechanism with force- or torque-controlled actuators, and using motion feedback, can be used to modulate output impedance. The actual output impedance consists of that due to the Proportional Derivative controller plus that due to the mechanism. This controller implements in robot joint space a dynamic behavior analogous to spring and damper. Manipulation tasks in unknown and unstructured environments can be better addressed with manipulators that are capable of force-sensing and controlling the end-effector impedance. A controller capable of adjusting on-line finger joint stiffness is able to execute robust grasp. Low impedance increases the mechanical robustness of the hand, as it permits safe operation of the hand in unknown environments. On the contrary, controlled high impedance permits the grasping of objects with different shapes and sizes and ensures the stability of a multi-fingered grasp against external disturbances of unknown intensity.

### 3.8. The CEA dexterous hand in the context of state-of-the-art tendon-driven hands

In this section we put the CEA dexterous hand in the context of state-of-the-art tendon-driven hands. The most defining design features, namely tendon routing and actuation architecture, are contrasted with those of the hand of the DLR Hand Arm System (Gebensteiner et al., 2010a, 2012). First, it must be clarified that both hands follow different design philosophies. The CEA hand exploits backdrivability and low mechanical impedance, while the DLR Hand uses non-backdrivable drive trains together with compliance mechanisms that absorb energy during impacts and are able to save energy to enhance the joint dynamics.

Both hands have a different number and distribution of DoFs, as well as different actuation architecture. The CEA hand has 20 DoFs distributed as explained in Section 2. Flexion/extension DoFs (i.e. distal joint of the thumb and kinematically coupled distal two joints of the fingers) are actuated by mono-directional actuators in opposition to passive return elements (Figure 4a). The rest of DoFs are actuated by bi-directional actuators (Figure 4b). Thus, there are 20 actuators, one motor per each DoF. In contrast, the DLR hand has 19 DoFs actuated by 38 actuators in such

a way that each DoF is actuated antagonistically using two actuators and two elastic elements.

In the CEA hand, all actuators are placed within the palm and the thumb base. Thus, the length of the tendons does not exceed a few centimeters, providing a high tendon stiffness which model-wise are considered as inelastic tendons (Figure 6). Besides, the passive return elements are realized by springs which model-wise are considered as elastic tendons of constant and known stiffness (Figure 7). Overall, the CEA hand uses a combination of inelastic and elastic force transmitting elements that minimizes the number of tendons and simplifies the cable routing (Section 3.3), ensuring simple, low-friction and low-impedance mechanics. In contrast, in the DLR hand all actuators are placed in the forearm, and thus each tendon length and its serial elasticity is modeled to adjust the stiffness-to-deflection characteristic, together with the mentioned compliance mechanisms.

In a similar way as shown in previous work (Martin et al., 2011), in the CEA hand joint stiffness can be adjusted by tuning the gains of the corresponding motor controller. Ongoing work is being done to quantify the reach of this approach. A mechanical limitation already exists, obviously, in the extension movement of the fingers, which is driven by the passive return spring in opposition to the backdrivable actuator. In the DLR hand, joint stiffness is adjusted by the antagonistic actuation of variable stiffness drives.

In the CEA hand, tendon routing and spring arrangement is designed to exactly eliminate the kinematic and static couplings between the abduction/adduction movement and the proximal/distal flexion/extension movements. In the DLR hand, this problem is addressed by passing the flexion/extension tendons nearly through the rotation center of the abduction/adduction joint.

Finally, in order to minimize friction the CEA hand totally eliminates tendon sliding from design. This is possible thanks to the novel tendon routing and the proximity of each actuator to the corresponding joint. The friction is minimized in the DLR hand by guiding the tendons via sliding surfaces which are machined out of low friction bearing plastics. This appears for example in the flexion/extension tendons passing through the abduction/adduction joint.

## 4. Experimental tests

### 4.1. Decoupling of the DoFs

As explained in preceding sections, a key design feature of the three-axes unit is the tendon routing, which minimizes kinematic and static coupling between the different axes. This allows the use of simple controller architecture which reduces the complexity associated with multi-input/multi-output (MIMO) control schemes. In this section, the decoupling of the DoFs is experimentally quantified in the low-frequency spectrum.

Extra position sensors have been temporarily mounted on each three-axes unit joint to record the three joint angles  $\theta$ . For each experiment, one motor is controlled in position while the other two motors are left free to move. First, the maximum cross couplings in quasi-static operations between abduction/adduction motions (around axis 1) and both proximal and distal flexion/extension motions (around axes 2 and 3) are below  $-28$  dB (Figure 14). Then, second, the maximum cross couplings between distal flexion/extension motion (around the axis 3) and the other two motions (around axes 2 and 3) are below  $-39$  dB (Figure 15).

According to the kinematic equations derived for the tendon transmission, these open-loop experimental characterizations ensure that the influence of the residual kinematic coupling effects are negligible in practice. Simple decentralized SISO control strategies can be advantageously exploited at low-frequency.

### 4.2. Backdrivability of the actuators

As explained above, the design driver of mechanical backdrivability improves natural mechanical behavior by permitting accurate feed-forward force control in the face of disturbances, enhances stable control of contact forces and, in general, safe robotic operation in unstructured environments. Impediments to backdrivability are friction and inertia in the mechanism. Acceleration-dependent backdrivability is guaranteed by a correct matching of the reduction ratios, but friction-dependent backdrivability needs to be determined. To this purpose, experimental tests were performed on the Steinmeyer Type B (3 mm x 1 mm) ball-screw, which is the key element to the backdrivability of the actuators.

Experimental setup is described next. The induced displacement of the ball-screw nut is transmitted by a tendon to drive a pulley which is loaded with different weights which produce a resisting torque in static equilibrium. The objective of the tests is to measure the performance of the ball-screw as a mechanical transmission both in the direct and reverse sense of the movement. Direct sense means the transmission from the motor (input torque) to the load (output force), and reverse sense means the transmission from the load (input force) to the motor (output torque).

Test were performed as follows:

1. The motor is fed with zero current.
2. The load is increased and the pulley starts rotating.
3. Motor current is increased until the pulley stops rotating. The value is noted for the reverse sense characterization.
4. Motor current is further increased until the pulley starts rotating in the opposite sense. The value is noted for the direct sense characterization.
5. The procedure is repeated for different values of the load.

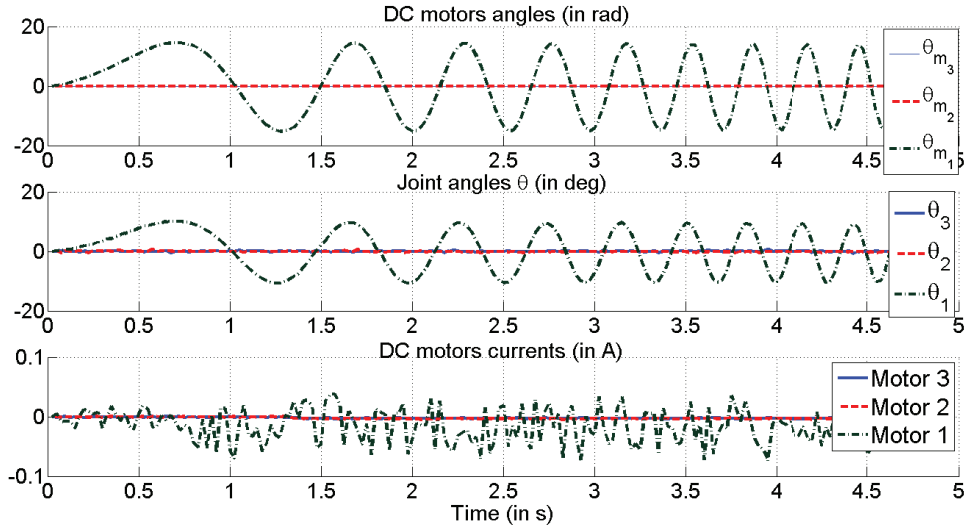


**Fig. 14.** Experimental evaluation of the abduction/adduction motion decoupling for a range of frequencies from 0.3 Hz to 3.0 Hz.

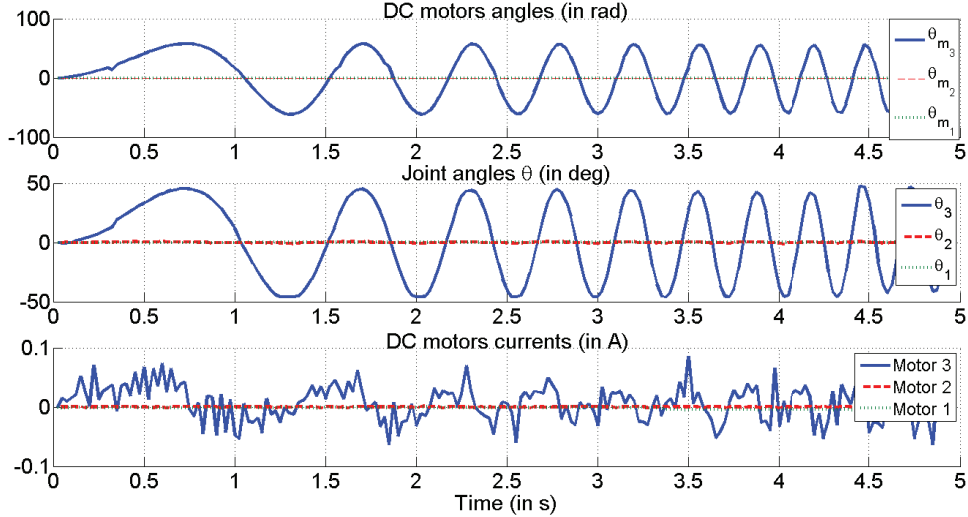


**Fig. 15.** Experimental evaluation of the distal flexion/extension motion decoupling for a range of frequencies from 0.3 Hz to 3.0 Hz.

Figure 16 shows experimental measures for both senses of transmission. The intersection with the  $x$ -axis gives the threshold of motor torque which initiates the movement. This *direct threshold* is 0.273 mNm. The intersection with the  $y$ -axis gives the threshold of external load which initiates the movement. This *reverse threshold* is 2.01 N. The low reverse threshold indicates that very little loads can be detected by current sensing in the motor; to give an idea, this value is equivalent to a 45gr threshold on the fingertip. From relationship (1) and using conservation of energy, the equivalent of loads at the motor shaft can be calculated. Then both direct and reverse efficiency of the transmission can be calculated, yielding values of 0.793 and 0.803 respectively. The high reverse efficiency indicates that the image of the load, seen from the motor, is not much perturbed by energy losses in the ball-screw transmission.

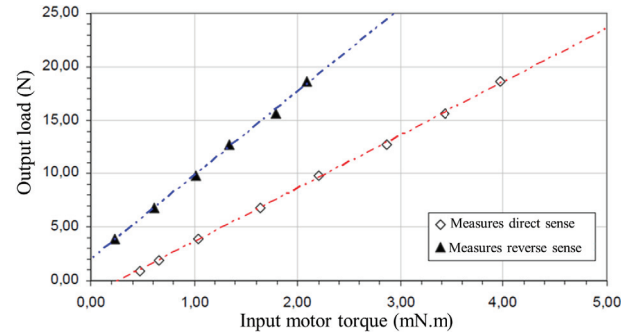


**Fig. 16.** Experimental measures on the ball-screw backdrivability.

#### 4.3. Backdrivability and contact force sensing

As previously explained in Section 2.2, our hand design permits us to obtain an estimate of the joint torques. Moreover, if the contact point is located by an additional sensing

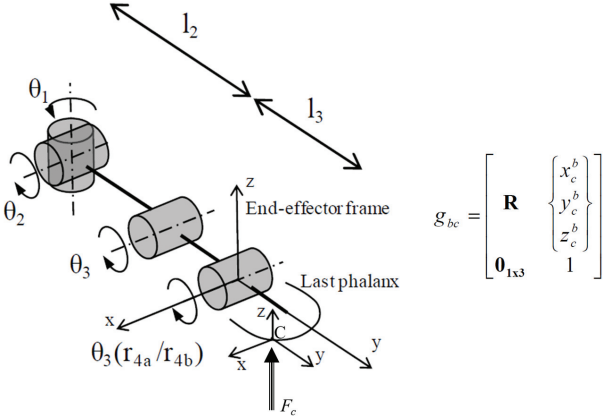


**Fig. 17.** Kinematics of the three-axes unit with contact force representation ( $g_{bc}$  denotes the forward kinematics transformation from the contact frame to the end-effector frame attached to the last phalanx).

device, it is then possible to obtain an estimate of the contact forces, which greatly improves the sensory capabilities of the hand.

**4.3.1. Contact force estimate.** The configuration-dependent body manipulator Jacobian matrix  $J_{st}^b(\theta)$  relates wrenches applied at the end-effector  $F_t$  and resulting joint torques  $\tau_F$  (Murray et al., 1994). Besides, the force applied by a contact is modeled as a wrench  $F_c$  applied at the origin of the frame  $C$  located at the contact point. Figure 17 illustrates this for the case of a contact point located in the last phalanx: end-effector frame B associated with the phalanx where the contact takes place. Mapping from frame C to frame B is given by  $g_{bc}$ , built from the rotation matrix  $R$  and the contact point coordinates with respect to the end-effector frame  $[x_c^b, y_c^b, z_c^b]^T$ . A wrench applied at the origin of the contact frame is mapped to a wrench applied at the end-effector frame by the following expression

$$F_t = Ad_{gbc}(\theta)^{-T} F_c \quad (15)$$

in which  $Ad_{gbc}$  represents the adjoint transformation associated with  $g_{bc}$ . For the case of contact point in the last phalanx, the joint torques that produce a desired contact wrench applied to the object are given by

$$\tau_F(\theta) = J_{st}^b(\theta)^T Ad_{gbc}(\theta)^{-T} F_c \quad (16)$$

In quasi-static operating modes, the inertial, Coriolis and centrifugal effects can be neglected, so that the equation of the finger dynamics in contact with a manipulated object simplifies into

$$\tau_F(\theta) = N(\theta, \dot{\theta}) - \tau_{act}(\theta, i) - \tau_{spr}(\theta) \quad (17)$$

where  $N(\theta, \dot{\theta})$  takes into account gravity and friction terms. The expression of the net joint torques  $\tau$  superposes the effects of the actuation  $\tau_{act}$  and spring efforts  $\tau_{spr}$ , as expressed in (12).

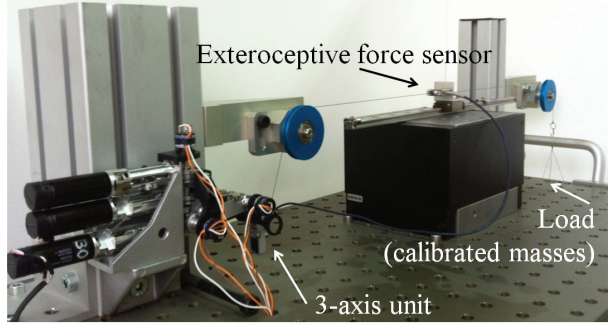


**Fig. 18.** Experimental test bench to contrast estimated and measured contact forces using exteroceptive force sensor.

The wrench  $F_c$  applied at the origin of the contact frame can be deduced combining (16) and (17). Based on sensorimotor information, all quantities except  $F_c$  can be computed on-line. Joint angles  $\theta$  can be estimated using (1) and (2) for slow motions.

**4.3.2. Sensitivity to contact forces.** By virtue of the backdrivability, contact forces exerted on the fingers induce torque perturbations at the motors level. When controlled in torque, motors ensure reference torque values at the output, resulting in a certain amount of finger displacement determined by the contact dynamics. The amount  $\|F_c\|$  of external force applied at the fingertip is then estimated from the strategy previously described. To validate this approach, an external force sensor has been used to have an external reference measure of the contact force for the experiments (Figure 18).

In the following, we assume that the contact point and thus the adjoint transformation associated with  $g_{bc}$  is a priori known from the experiment design. Likewise, all joint angles are measured and thus the body manipulator Jacobian matrix  $J_{st}^b(\theta)$  can be calculated. Calibrated masses are used as external loads acting as a counterweight in a cable-pulley arrangement which transmits the weight of the masses to the contact point on the distal phalanx of the finger. The exteroceptive force sensor (Futek LSB200) measures the tension of the cable, and thus the force applied at the contact point. To simplify the firsts experiments, only the two distal joints are free to move; the remaining joints have been blocked by mechanical stops added for the experiment. This way, only one motor is used for the purpose of contact force estimate, which is controlled in torque. When the motor is given a step torque reference, the joint undergoes a certain displacement and contact forces are measured. Different contact forces are obtained through different values of the calibrated masses.

Figures 19 and 20 show experimental results for external loads of 0.6N and 1N. The timescale is common to all Figures. At  $t = 0$ , a step reference is given to the motor current controller. At  $t_i$ , a certain amount of mass is added

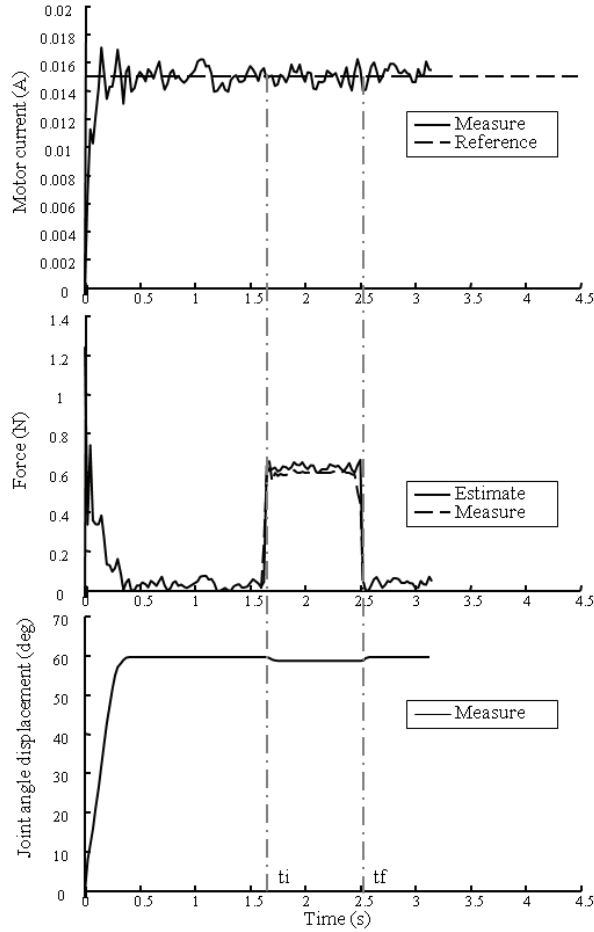


**Fig. 19.** Experimental results of the estimate of contact forces compared with an exteroceptive force sensor for a load of 0.6 N.

to the counterweight, and at  $t_f$  it is removed, both manipulations in quasi-static conditions. Figure 19 (*top*) shows the motor current following the step reference throughout the whole experiment; *bottom* shows a certain displacement of the measured joint angle; and *middle* superposes the measured and the estimated contact forces, caused by an external load of 0.6 N. Figure 20 shows the same experiment for an external load of 1 N.

The lowest contact force detected was about 0.4 N, which indicates the contact force sensitivity threshold of the measuring strategy. In a recent review of tactile sensing for robotic dexterous in-hand manipulation, Yousef et al. (2011) proposes a force sensitivity range of 0.01 – 10 N as a design guideline. This is a promising result that validates our sensing approach and its potential complementarity with tactile skin sensing solutions, as discussed in Section 2.2. Extensive experimentation is being carried out on the contact force estimate for different finger configurations and combinations of active motors.

#### 4.4. Grasping abilities

The grasping performance of the hand of the new CEA dexterous hand is being evaluated with some first tests.

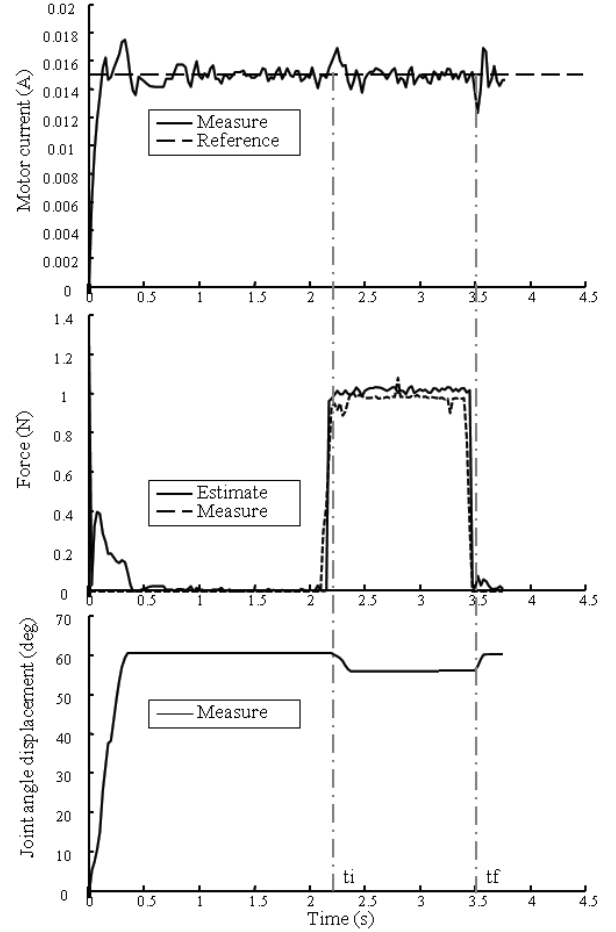


**Fig. 20.** Experimental results of the estimate of contact forces compared with an exteroceptive force sensor for a load of 1 N.

Different types of grasps (Cutkosky, 1989) of everyday objects of different shapes and material properties have been carried out to evaluate the grasping performance of the hand. Figure 21 shows the prismatic power grasp of a plastic bottle, the trypod precision grasp of a light bulb, the sphere precision grasp of a ball, and the manipulation of a syringe. The robustness of the grasps against disturbances and the in-hand manipulation will be investigated in future work.

## 5. Conclusions and perspectives

A new hand has been presented which combines high levels of both anthropomorphism and dexterity. This design challenge has been addressed through the combination of three main mechanical design ideas: modularity, backdrivability and mechanical simplicity. Modularity is achieved by the design and optimization of a separable sub-assembly, the *three-axes unit*, which is then integrated in all fingers and the thumb. This greatly simplifies the inherent complexity of the 24 DoF assembly of the complete hand and ensures a better performance homogeneity of the different DoFs. Mechanical simplicity is further achieved by a new

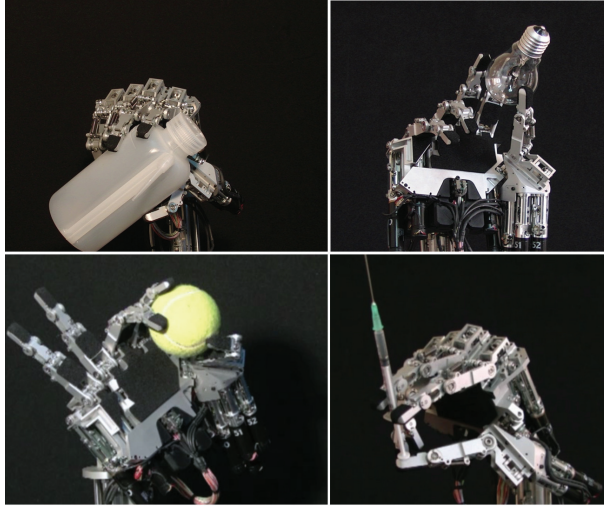


**Fig. 21.** Grasps of various objects using the CEA dexterous hand.

transmission design which minimizes kinematic and static coupling between DoFs, further simplifying the low-level control of the hand.

Backdrivability is addressed at both actuator and transmission level. Backdrivable actuators consist of a rotary DC motor coupled to a ball-screw rotary-to-linear transmission. Motor output and ball-screw reduction ratio are chosen to simultaneously obtain a sufficient actuator output and a maximum acceleration-dependent backdrivability. For the mechanical transmission a new design is presented which minimizes the number of idle pulleys and direction changes in the tendon routing, maximizing friction-dependent backdrivability.

Overall, the mechanical advantages of the proposed design have a direct impact in the controllability of the mechanism, which in turn enhances the dexterity of the hand.

A thorough discussion has been presented regarding the impact of backdrivability on the control, sensing and safety of the hand, identifying the design tradeoffs. Backdrivability enhances the dexterity related to the sensory apparatus of the hand, as it permits contact force estimate through motor current measure and contact point measure. In this way, every surface becomes sensitive as every part of the hand is driven by a backdrivable actuator. Even if the information provided by this approach is not complete, we believe it is a complementary solution that could help compensate for the technical difficulty of realizing a sufficiently functional artificial skin. In addition, backdrivability also opens new possibilities for compliance control, which improves stability of a multi-fingered grasp against external disturbances of unknown intensity.

Experimental results validate the design approach and the theoretical performance. This encourages the authors to follow this research line and further investigate new control and sensing strategies enabled by the backdrivable mechanical design. Exhaustive experimentation is being carried

out on the compliance control and further steps would involve high-level control of the complete hand to achieve dexterous in-hand manipulation.

### Acknowledgements

The authors wish to thank Florian Gosselin for advice on actuation architecture design, as well as Tanguy Jouan-De-Kervenoael and Benoit Perochon for help with prototype manufacturing.

### Funding

This work was supported by the HANDLE project, which has received funding from the European Community Seventh Framework Program (FP7/2007-2013; grant number ICT 231640).

### References

- Albu-Schäffer A, Haddadin S, Ott CH, et al. (2007) The DLR lightweight robot: Design and control concepts for robots in human environments. *Industrial Robot: An International Journal* 34(5): 376–385.
- Albu-Schäffer A, Eiberger O, Grebenstein M, et al. (2008) Soft robotics: From torque feedback controlled lightweight robots to intrinsically compliant systems. *IEEE Robotics and Automation Magazine* 15: 20–30.
- Ambrose RO, Aldridge H, Askew RS, et al. (2000) Robonaut: Nasa's space humanoid. *IEEE Intelligent Systems* 1: 57–63.
- Baker BS, Fortune S and Grosse E (1985) Stable prehension with a multi-fingered hand. In: *IEEE International conference on robotics and automation*, Durham, UK, March 1985, pp. 570–575.
- Biagiotti L, Lotti F, Melchiorri C and Vassura G (2004) How far is the human hand? A review on anthropomorphic robotic end-effectors. Technical Report, University of Bologna, Italy.
- Bicchi A (2000) Hands for dexterous manipulation and robust grasping: A difficult road toward simplicity. *IEEE Transactions on Robotics and Automation* 16(6): 652–662.
- Bitzer S and Smagt P (2006) Learning EMG control of a robotic hand: Towards active prostheses. In: *IEEE International conference on robotics and automation*, Orlando, FL, 15–19 May 2006, pp. 2819–2823.
- Butterfaß J, Grebenstein M, Liu H and Hirzinger G (2001) DLR-hand II: Next generation of a dextrous robot hand. In: *IEEE International conference on robotics and automation*, Seoul, South Korea, 21–26 May 2001, pp. 109–114.
- Chalon M, Friedl W, Reinecke J, Wimboeck T and Albu-Schaeffer A (2011) Impedance control of a non-linearly coupled tendon driven thumb. In: *IEEE/RSJ International conference on intelligent robots and systems*, San Francisco, CA, 25–30 September 2011, pp. 4215–4221.
- Chalon M, Grebenstein M, Wimböck T and Hirzinger G (2010) The thumb: Guidelines for a robotic design. In: *IEEE/RSJ International conference on intelligent robots and systems*, Taipei, 18–22 October 2010, pp. 5886–5893.
- Cutkosky M (1989) On grasp choice, grasp models, and the design of hands for manufacturing tasks. *IEEE transactions on robotics and automation* 5(3): 269–279.
- Cutkosky M and Kao I (1989) Computing and controlling the compliance of a robotic hand. *IEEE transactions on robotics and automation* 5: 151–165.

- Dias J, Lobo J, Trindade P and Perdereau V (2012) Workshop introductory tutorial to ROS and its use for robot in-hand manipulation. In: *IEEE/RSJ International conference on intelligent robots and systems*, Algarve, Portugal, 7–12 October 2012.
- Dollar AM and Howe RD (2010) The highly adaptive SDM hand: Design and performance evaluation. *International Journal of Robotics Research* 29(5): 585–597.
- Doulgeri Z and Arimoto S (2002) A position/force control for a robot finger with soft tip and uncertain kinematics. *Journal of Robotic Systems* 19(3): 115–131.
- Doulgeri Z and Karayannidis Y (2005) Robot in compliant contact with an unknown surface. In: *IEEE International conference on robotics and automation*, Barcelona, Spain, 18–22 April 2012, pp. 2696–2701.
- Fischer T and Woern H (1998) Structure of a robot system: Karlruhe dexterous hand II. In: *6th IEEE Mediterranean conference on control and systems*, Alghero, Italy, 9–11 June 1998, pp. 765–770. IEEE.
- Gazeau J, Zeghloul S, Arsicault M and Lallemand J (2001) The LMS hand: Force and position controls in the aim of the fine manipulation of objects. In: *IEEE International conference on robotics and automation*, Seoul, South Korea, 21–26 May 2001, pp. 2642–2648.
- Goldenberg A (1988) Implementation of force and impedance controlling robot manipulators. In: *IEEE International conference on robotics and automation*, pp. 1616–1632.
- Grebenstein M, Albu-Schäffer A, Bahls T, et al. (2011) The DLR hand arm system. In: *IEEE International conference on robotics and automation*, Philadelphia, PA, 24–29 April, pp. 3175–3182.
- Grebenstein M, Chalon M, Friedl W, et al. (2012) The hand of the DLR hand arm system: Designed for interaction. *The International Journal of Robotics Research* 31(13): 1531–1555.
- Grebenstein M, Chalon M, Hirzinger G and Siegwart R (2010a) Antagonistically driven finger design for the anthropomorphic DLR hand arm system. In: *IEEE-RAS International conference on humanoid robots*, Nashville, TN, 6–8 December, pp. 609–616.
- Grebenstein M, Chalon M, Hirzinger G and Siegwart R (2010b) A method for hand kinematics designers 7 billion perfect hands. In: *1st International conference on applied bionics and biomechanics*, Venice, Italy, 14–16 October 2010.
- Haddadin S, Parusel S, Belder R, Albu-Schäffer A and Hirzinger G (2011) Safe acting and manipulation in human environments: A key concept for robots in our society. In: *IEEE ARSO: A Workshop in advanced robotics and its social impacts*, Half-Moon Day, CA, 2–4 October 2011, pp. 72–75.
- Hanafusa H and Asada H (1997) Stable prehension by a robot hand with elastic fingers. In: *7th International symposium on industrial robots*, Tokyo, Japan, pp. 361–368.
- He P, Jin MH, Yang L, et al. (2004) High performance DSP/FPGA controller for implementation of HHIT/DLR dexterous robot hand. In: *IEEE International conference on robotics and automation*, New Orleans, LA, 26 April–1 May 2004, pp. 3397–3402.
- Hirzinger G, Butterfaß J, Fischer M, et al. (2000) A mechatronics approach to the design of light-weight arms and multifingered hands. In: *IEEE International conference on robotics and automation*, San Francisco, CA, 24–28 April 2000, pp. 46–54.
- Hogan N (1985) Impedance control: An approach to manipulation: Part I—Theory. *Journal of Dynamic Systems, Measurement, and Control* 107(1): 1–7.
- Hoshino K and Kawabuchi I (2005) Stable pinching with fingertips in humanoid robot hand. In: *IEEE/RSJ International workshop on intelligent robots and systems*, Edmonton, Canada, 2–6 August 2006, pp. 3815–3820.
- Jacobsen SC, Iversen EK, Knutti DF, Johnson RT and Biggers KB (1986) Design of the Utah/M.I.T. dexterous hand. In: *IEEE International conference on robotics and automation*, Orlando, FL, 15–19 May, pp. 1520–1532.
- Jau BM (1995) Human-like compliance for dexterous robot hands. In: *IFTOM 9th world congress on the theory of machines and mechanisms*, Milan, Italy, 29 August–2 September 1995, pp. 2239–2243.
- Jung S, Hsia T and Bonitz R (1999) Force tracking impedance control of robot manipulators under unknown environment. *IEEE Transactions on Control Systems Technology* 44(4): 798–802.
- Kaneko K, Harada K and Kanehiro F (2007) Development of multi-fingered hand for life-size humanoid robots. In: *IEEE International conference on robotics and automation*, 10–14 April 2007, Rome, pp. 913–920.
- Kawasaki H, Komatsu T and Uchiyama K (2002) Dexterous anthropomorphic robot hand with distributed tactile sensor: GIFU hand II. *IEEE/ASME Transactions on Mechatronics* 7(3): 296–303.
- Kazerooni H, Sheridan T and Houpt P (1986) Robust compliant motion for manipulators: Part I—The fundamental concepts of compliant motion; Part II—Design method. *IEEE Journal of Robotics and Automation* 2(2): 83–105.
- Kerr J and Roth B (1986) Analysis of multifingered hands. *International Journal of Robotics Research* 4(4): 3–17.
- Koganezawa K, Kunugi N and Niikura R (2011) Backdrivable mechanism for artificial finger. In: *18th IFAC world congress*, Milan, Italy, 28 August–2 September 2011, pp. 8095–8100.
- Liu H, Wu K, Meusel P, Seitz N, Hirzinger G and Jin M (2008) Multisensory five-finger dexterous hand: The DLR/HIT hand II. In: *IEEE/RSJ Workshop on Intelligent Robots and Systems*, pp. 3692–3697.
- Lotti F, Tiezzi P, Vassura G, et al. (2005) Development of UB hand 3: Early results. In: *IEEE International conference on robotics and automation*, Nice, France, 22–26 September 2005, pp. 4499–4504. IEEE.
- Maekawa H, Yokoi K, Tanie K, Kaneko M, Kimura N and Ima-mura N (1992) Development of a three-fingered robot hand with stiffness control capability. *Mechatronics* 5(5): 483–494.
- Martell JWS and Gini G (2007) Robotic hands: Design review and proposal of new design process. *International Journal of Applied Mathematics and Computer Science* 4(2): 587–592.
- Martin J, Huard B, Robert M and Grossard M (2011) Design of a novel self-sensing and compliance controlled robotic finger joint. In: *IEEE/ASME International conference on advanced intelligent mechatronics*, Budapest, Hungary, 3–7 July 2011, pp. 1520–1532.
- Matsuoka Y, Afshar P and Oh M (2006) On the design of robotic hands for brain-machine interface. *Neurosurgical Focus* 20(5): 1–9.
- Melchiorri C and Kaneko M (2008) Robot hands. In: Siciliano B and Khatib O (eds) *Springer Handbook of Robotics*. Berlin: Springer-Verlag, pp. 345–360.

- Murray RM, Li Z and Sastry SS (1994) *A mathematical Introduction to Robotic Manipulation*. CRC Press.
- Namiki A, Imai Y, Ishikawa M and Kaneko M (2003) Development of a high-speed multifingered hand system and its application to catching. In: *IEEE/RSJ workshop on intelligent robots and systems*, Las Vegas, NV, 27–31 October 2003, pp. 2666–2671.
- Okada T (1986) Computer control of multijointed finger system for precise object handling. In: Pham DT and Hegbinbotham WB (eds) *International Trends in Manufacturing Technology: Robot Grippers*. Berlin: Springer-Verlag, pp. 391–417.
- Roccella S, Carrozza MC, Cappiello G, et al. (2004) Design, fabrication and Preliminary results of a novel anthropomorphic hand for humanoid robotics: RCH-1. In: *IEEE/RSJ workshop on intelligent robots and systems*, Sendai, 28 September–2 October, pp. 266–271.
- Salisbury JK and Craig JJ (1982) Articulated hands: Force control and kinematic issues. *The International Journal of Robotics Research* 1(1): 4–17.
- Salisbury JK and Roth B (1983) Kinematics and force analysis of articulated mechanical hands. *Journal of Mechanisms, Transmissions and Actuation in Design* 135: 35–41.
- Salisbury JK and Ruoff C (1981) The design and control of a dexterous mechanical hand. In: *ASME computer conference*, Minneapolis, MN.
- ShadowRobotCompany (2013) Shadow dexterous hand tech spec E1 series. Available at: [www.shadowrobot.com](http://www.shadowrobot.com).
- Townsend W and Salisbury J (1989) Mechanical bandwidth as a guideline to high-performance manipulator design. In: *IEEE International conference on robotics and automation*, Scottsdale, AZ, 14–19 May 1989, pp. 1390–1395.
- Ueda J, Kondo M and Ogasawara T (2010) The multifingered NAIST hand system for robot in-hand manipulation. *Mechanism and Machine Theory* 45: 224–238.
- Yamano I, Takemura K and Maeno T (2003) Development of a robot finger for five-fingered hand using ultrasonic motors. In: *IEEE/RSJ workshop on intelligent robots and systems*, Las Vegas, NV, 27–31 October 2003, pp. 2648–2653.
- Yousef H, Boukallel M and Althoefer K (2011) Tactile sensing for dexterous in-hand manipulation in robotics—A review. *Sensors and Actuators A: Physical* 167: 171–187.